

Saturation of fishbone modes by self-generated zonal flows in tokamak plasmas

G. Brochard, C. Liu, X. Wei, W. Heidbrink, Z. Lin, N. Gorelenkov,
S.D. Pinches, P. Liu, J. H. Nicolau, H. Lütjens

Abstract

Gyrokinetic and kinetic-MHD simulations of $n=1$ fishbone modes in DIII-D plasmas find that self-generated zonal flows can dominate the fishbone saturation. The saturation mechanism is identified in phase space, where the zonal flows prevent holes and clumps from persisting or drifting in phase space with mode down-chirping, reducing the wave-particle resonant drive. This saturation is confirmed by quantitative agreement with experimental measurements for both mode saturation amplitude and neutron emissivity. Zonal flows shearing rate exceeds the drift-wave growth rate, consistent with the ITB observed in DIII-D plasmas. The deliberate destabilization of fishbones for the development of high performance scenarios in ITER is then proposed.

Introduction. - Energetic Particles (EPs) in tokamak plasmas can destabilize a large spatial range of instabilities that may lead to their outward transport. This is a critical issue for burning plasmas as in ITER [1] since such a transport can degrade the fusion performances, the plasma confinement as well as threaten the reactor's integrity. This transport therefore needs to be predicted for mitigation strategies to be incorporated in plasma scenarios.

Fortunately, it was discovered theoretically [2][3][4][5] and shown numerically [6][7][8][9][10] that instabilities arising at the microscopic and mesoscopic scales such as drift-waves and Alfvén eigenmodes (AEs) are able to excite zonal flows (ZFs), that can mitigate the saturation amplitudes of these modes, and therefore the associated EP transport. Besides this mitigation, the destabilisation of zonal flows can generate strongly sheared poloidal flows that suppress turbulent transport by damping drift-waves turbulence [11], resulting in the formation of an internal transport barrier (ITB) that greatly enhances plasma confinement [12][13]. Macroscopic MHD modes triggered by energetic particles such as the fishbone instability [14][15] however were not self-consistently observed to trigger $n = m = 0$ zonal flows so far. The mechanism dominating the fishbone saturation was identified in nonlinear simulations [16][17][18][19] to be the resonant wave-particle trapping due to kinetic nonlinearities, mode-mode nonlinearities playing a secondary role.

In this Letter, we report the first self-consistent gyrokinetic simulations finding fishbone saturation by the self-generated zonal flows, in a DIII-D discharge. This discharge is chosen for validation purposes to predict the EP transport in a ITER baseline prefusion scenario [20]. The zonal flows are found to be force-driven by the fishbone and are the main mechanism for the fishbone saturation. This mechanism is

observed for the first time in phase space, where zonal flows prevent hole and clump structures from persisting or drifting in the nonlinear phase, reducing the EP resonant drive. This saturation by zonal flows is confirmed by experimental measurements, as simulations including zonal flows are able to recover quantitatively, for the first time, the mode saturation amplitude and the neutron emissivity drop. Moreover, the shearing rate generated by the fishbone-induced zonal flows exceeds the linear growth rate of unstable drift-wave modes, similar to recent numerical work based on EAST discharges [21]. This strong $E \times B$ suppression is consistent with the ITB arising experimentally after fishbone bursts in the DIII-D discharge. It confirms the long suspected role of fishbones in ITB formation [22], fishbone bursts having been observed to precede ITBs in ASDEX [23], MAST [24][25], HL-2A [4] and EAST [26][27] plasmas. Finally, gyrokinetic simulations find that the fishbone-induced EP transport in the ITER scenario is marginal, 2% of the core EPs being redistributed, similar to previous studies on the alpha fishbone in ITER DT scenarios [19]. The intentional destabilization of fishbone modes in ITER scenarios is therefore possibly a way to enhance fusion performances.

Experimental setup. - The selected DIII-D discharge #178631 [28] has a nearly circular oval shape (elongation $\kappa = 1.17$, triangularity $\delta = 0.07$) that is limited on the carbon inner wall. The major radius is $R_0 = 1.74$ m, the minor radius is $a = 0.64$ m, the toroidal field is 2.0 T, the plasma current is 0.88 MA, and the line-average electron density is $\sim 2.0 \times 10^{19} \text{ m}^{-3}$. This discharge was chosen primarily because it has an accurately known, weakly reversed, q profile with $q_0 = 1.2$, $q_{min} = 1.09$, and $q_{95} = 3.8$ values that resemble the profile predicted for the ITER baseline scenario. The deuterium, L-mode plasma is heated by 3.8 MW of 81

keV deuterium beams that are injected in the midplane in the direction of the plasma current and by 1.0 MW of 2nd harmonic, central electron cyclotron heating.

Numerical setups. - The DIII-D discharge #178631 is studied numerically mostly through gyrokinetic simulations with the GTC code [6][29][30][31], and with kinetic-MHD simulations using the M3D-C1 [32][33][34] and XTOR-K [35][36][37] codes. GTC capability at simulating MHD modes was recently verified and validated on DIII-D experiments [38]. The magnetic configuration is reproduced from the EFIT code at $t=1580\text{ms}$. Plasma profiles are obtained from TRANSP simulations. To simulate properly MHD modes, the sum of partial pressures need to add up to the total pressure in EFIT, which is not always the case using TRANSP profiles. To ensure it, the EP pressure is constrained as $p_f = p_{tot} - p_i - p_e$, given that the uncertainty on EP profiles in TRANSP is the highest. The experimental NBI distribution is reproduced from the NUBEAM code. Such a distribution is described in our first-principle simulations with an anisotropic slowing-down model, using a zero-th order Legendre expansion [39]. A superposition of three slowing-downs is used to reproduce the injection energies at nominal, half and third energies. The critical velocity is artificially set to recover similar gradients in the $(E, v_{||}/v)$ phase space. All nonlinear simulations cover the whole simulation domain, with an edge buffer after $\rho_T = \sqrt{\psi_T/\psi_{T,\text{edge}}} = 0.8$ in GTC suppressing equilibrium gradients. GTC retains only the $n=1$ mode in its simulations, with or without the $n=m=0$ zonal component, using kinetic thermal/fast ions and fluid electrons. M3D-C1 covers low n modes $n \in [0, 2]$ with both thermal and fast ions kinetic effects. Due to the anisotropic nature of the chosen configuration that has $\beta_f/\beta_{tot} = 54\%$ on axis, XTOR-K only evolves the $n=1$ mode, as the $n=0$ mode contains both equilibrium and perturbed fields in the code, contrarily to GTC and M3D-C1. XTOR-K treats kinetically only the fast ion species. Convergence studies over spatial grid size, time step and number of particles per cell were successfully conducted.

Fishbone mitigation by self-induced zonal flows - The impact of MHD nonlinearities on the $n=1$ fishbone were previously examined numerically by keeping side-band $n=0-4$ modes, highlighting reduction of initial saturation amplitude [18][21], and generation of $n=m=0$ sheared poloidal flows [19][21]. The role played specifically by zonal flows in fishbone mitigation was however not identified. The effects of zonal flows on the fishbone instability are studied here self-consistently for the first time with the gyrokinetic GTC code. A gyrokinetic treatment of zonal flows is essential as it takes into account their collisionless damping [40], which is absent in the kinetic-MHD formalism without kinetic thermal ions effects. For the considered DIII-D configuration, a $n=1$ fishbone mode is linearly unstable, close to marginal stability at $p_{f,\text{thres}} = 0.8p_f$, with a growth rate of

$\gamma_{n=1} = 8.5 \times 10^4 \text{ s}^{-1}$ and a mode frequency of $\omega/2\pi = 17\text{kHz}$ in GTC simulations.

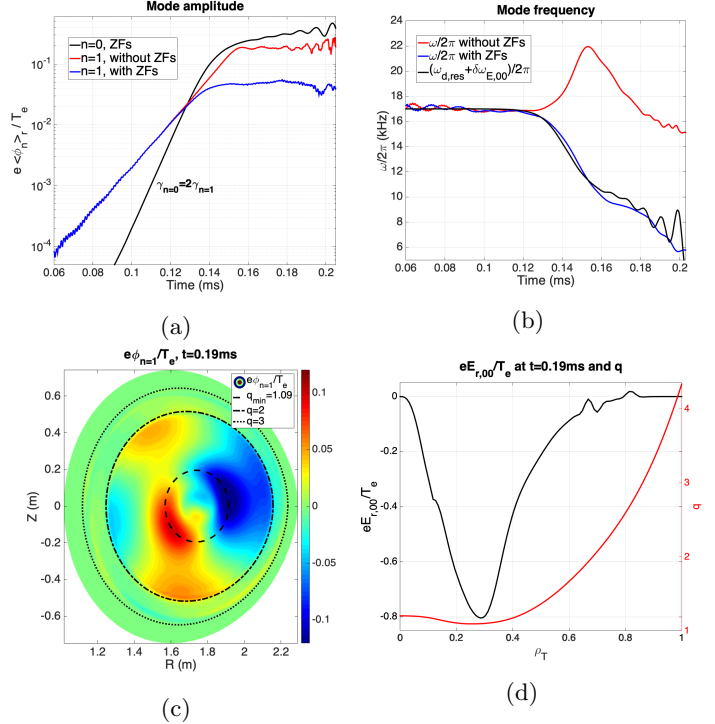


Figure 1: Time evolution of (a) the volume-averaged perturbed electrostatic potential $e\phi/T_e$ ($n=0,1$), and (b) the $n=1$ mode frequency ω , with and without zonal flows in GTC simulations. The linearly resonant precessional frequency plus the zonal $E \times B$ frequency is also displayed. (c) $e\phi/T_e$ mode structure in the poloidal plane after mode saturation. (d) Zonal electric field $eE_{r,00}/T_e$ after mode saturation.

When the realistic beam is replaced by its equivalent Maxwellian distribution, this mode is fully stabilized, highlighting the sensitivity of fishbone instabilities over EP distributions.

Nonlinear simulations are performed with and without the $n=m=0$ component, as illustrated in Fig.1. The time evolution of the volume-averaged electrostatic potential $e\phi/T_e$, displayed on Fig.1a, shows that the $n=1$ fishbone mode is able to force-drive the $n=m=0$ zonal flow, with a growth rate twice that of the $n=1$. As shown analytically in [5] for TAEs, the mechanism for this zonal flow generation is the charge separation induced by nonlinear EP redistribution, as opposed to the usual one relying on Reynolds and Maxwell stresses [2][3][4][9]. As the $n=0$ amplitude exceeds the $n=1$ at $t=0.13\text{ms}$, the zonal mode forces the fishbone to

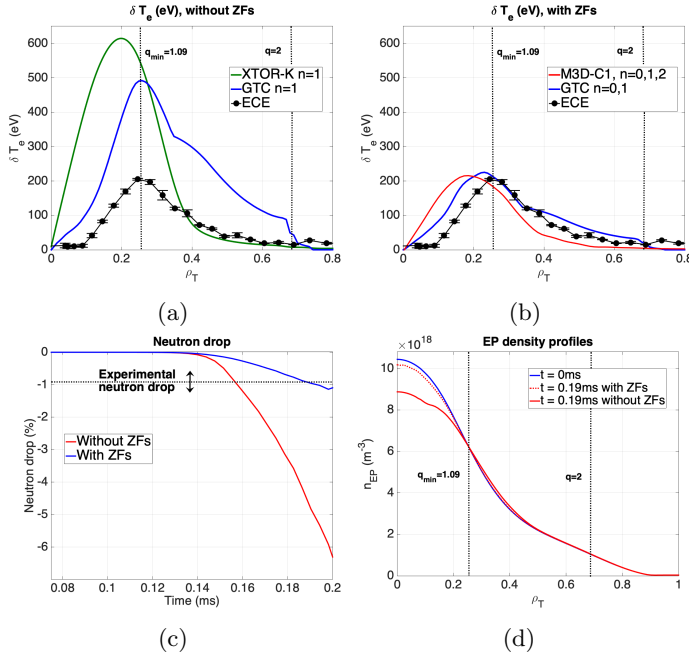


Figure 2: Radial envelope of δT_e after saturation without (a) and with (b) zonal flows in GTC, M3D-C1 and XTOR-K simulations, compared to the ECE measurement for the DIII-D #178631 discharge. (c) Time evolution of the simulated neutron drop, with and without zonal flows. (d) EP density profiles in GTC simulations before and after fishbone burst.

saturate at $\delta B/B_0 \sim 2 \times 10^{-3}$, with a saturation amplitude lower by a factor of 4 compared to the case without zonal flows. The zonal flows saturates at an even larger amplitude, about six times larger than the $n=1$ mode when including zonal flows, with a spontaneous growth after $t=0.15\text{ms}$ when the $n=1$ is fully saturated. Such mitigation by zonal flows have been theoretically predicted [2][3][5] and numerically observed [7][8][9][10] for Alfvén eigenmodes, but never so far for the fishbone instability. The zonal flows inclusion also lowers significantly the EP diffusivity at saturation, from 30 to $4 \text{ m}^2 \cdot \text{s}^{-1}$. As shown in Figure 1b, the mode frequency down-chirps after the $n=1$ mode saturation with and without zonal flows, which is a typical fishbone signature, with similar chirping rates. Just before saturation, the case without zonal flows experiences a notable up-chirping of the mode frequency, that stops when the mode starts saturating. This increase may be attributed to the larger mode amplitude near saturation. The $n=1$ electrostatic potential and the $n=0$ radial electric field after saturation at $t=0.19\text{ms}$ are displayed on Fig.1c-d. The $n=1$ mode features a dominant $m=1$ harmonic centered around q_{min} , as well as a significant $m=2$ side-band that vanishes after $q=2$. The zonal electric field exhibits a macroscopic structure centered near q_{min} as well, which differs from the usual mi-

croscopic/mesoscopic scale observed with drift-waves/AEs-induced zonal flows. This large structure can be attributed to the charge separation provoked by the outward drift of resonant EPs within the $n=1$ mode. It leads to a strongly sheared poloidal rotation in the electron direction, which is opposite to the $n=1$ fishbone rotation, and a weak toroidal rotation.

This fishbone mitigation by self-generated zonal flows is experimentally confirmed by DIII-D measurements as can be seen in Fig.2. The δT_e envelope obtained from GTC, M3D-C1 and XTOR-K nonlinear simulations at saturation are compared with the ECE measurements on Fig.2 (a-b), with and without zonal flows inclusion. The δT_e envelope is defined here as the $n=1$ sum of all poloidal harmonics. Without zonal flows, XTOR-K and GTC results have comparable saturation amplitudes with $\delta T_{e,max} \sim 500 - 600 \text{ eV}$, which are three time larger than the experimental saturation. The simulated envelopes differ however, GTC results having a dominant $m=2$ harmonic after $\rho = 0.34$. When including zonal flows however, M3D-C1 and GTC saturation amplitudes at $\delta T_{e,max} \sim 200 \text{ eV}$ match very well with the experimental one. The significant $m=2$ harmonic in GTC simulations leads to a quantitative agreement with the ECE measurement, which provides a nonlinear validation for GTC regarding fishbone instabilities, completing the linear one obtained in [38] for kink instabilities. Nonlinear scans for the fishbone saturation amplitude performed over the radial position and amplitude of q_{min} recover the same significant mitigation by zonal flows. This nonlinear validation is further demonstrated by comparing the simulated and experimental volume-averaged neutron emissivity. In GTC the volume-averaged neutron flux is defined as $\Gamma_N = n_i \sum_k^N \delta(\mathbf{x} - \mathbf{x}_{f,k}) \delta(\mathbf{v} - \mathbf{v}_{f,k}) \sigma(v_{f,k}) v_{f,k}$ with n_i the thermal ion density profile, x_k and v_k the position and velocity of EPs and σ the D-D nuclear fusion cross section, assuming reasonably that $v_i \ll v_f$. As shown on Fig.2c, without zonal flows GTC recovers a neutron drop at saturation of about 6%, much higher than the experimental one at $\delta \Gamma_N = 0.9\% \pm 0.3\%$. When including zonal flows however, the neutron drop yields $\delta \Gamma_N \sim 1.1\%$, which falls within the experimental interval. As expected from these neutron drop values, the fishbone-induced EP transport with zonal flows is rather weak as shown on Fig. 2d, with about 3% of EPs inside of the q_{min} volume redistributed outward. The redistribution is more significant without zonal flows, as it affects 15% of EPs in the core plasma.

Mechanism for fishbone mitigation by zonal flows - Beyond the additional dissipation brought by the inclusion of the $n=0$ toroidal mode [7], phase-space analysis reveals that zonal flows influence the time evolution of coherent phase space structures, impacting the $n=1$ fishbone mode saturation. On Fig.3, the instantaneous EP transport $\partial_t \delta f$ is displayed in the invariants phase space diagram ($P_\zeta, \lambda = \mu B_0/E$) at fixed magnetic momentum $\mu B_0 = 45\text{keV}$ before

and after the fishbone saturation, with and without zonal flows. The instantaneous transport is chosen rather than the usual perturbed EP distribution δf as the fishbone mode frequency is chirping in the nonlinear phase, which leads phase space structure to drift in time. In the linear phase, the mode is driven by two resonances, the precessional one $\omega = \omega_d$ linked to trapped particles, and a drift-transit one $\omega = \omega_\zeta - \omega_b$ due to passing particles, with $\omega_\zeta = q\omega_b + \omega_d$ the drift frequency and ω_b the bounce/transit frequency. The passing and trapped phase space zones are separated by a black line on the diagrams.

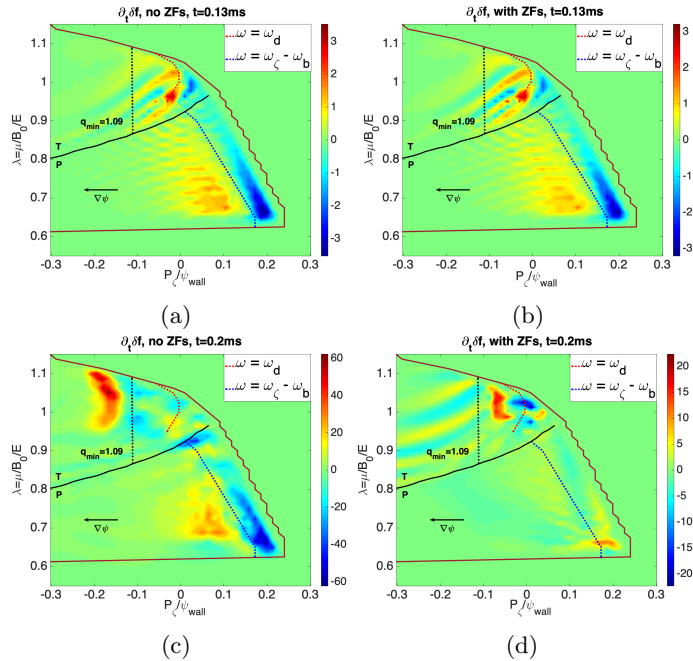


Figure 3: Time evolution of the instantaneous EP transport $\partial_t \delta f$ without (left) and with (right) zonal flows, in the invariants (P_ζ, λ) phase space diagram at fixed μ ($\mu B_0 = 45\text{keV}$).

As can be observed on Fig.3 (a-b), a hole and clump structure develops around each resonances in the linear phase, indicating a resonant outward EP redistribution. In the nonlinear phase, the dynamical evolution of these phase space structures differ significantly with and without zonal flows. In their absence, the hole and clump in the trapped region drifts to higher ψ positions, under the influence of the mode down-chirping as $\omega_d \propto 1/\psi$, while the one in the passing part does not move. However with zonal flows, the phase space structure in the trapped region remains static, even thought the mode is chirping down, and the hole and clump in the passing part vanishes. Such behaviours prevent the fishbone mode from affecting resonantly new EPs, which leads to its weaker saturation due to the absence of drive.

These differences in dynamical evolution can be explained by the influence of the zonal flows on the EPs wave-

particle resonance. The perturbed radial electric field associated with zonal flows generates an additional drift velocity $\delta \mathbf{v}_{E,00} = \delta \mathbf{E}_{00} \times \mathbf{B}/B^2$. This additional velocity leads to an $E \times B$ drift frequency defined in general geometry as $\omega_{E,00} = \langle \mathbf{v}_{E,00} \cdot (\nabla \zeta - q \nabla \theta) \rangle$ with $\langle \cdot \cdot \cdot \rangle$ the bounce-average operator, which yields $\delta \omega_{E,00} = \delta E_\psi = -\nabla \phi_{00}$ using a thin-orbit width approximation for simplicity. This is similar to the so-called "orbit-squeezing" effects in neoclassical theory [41], EPs have an overall decrease of their precessional frequency due to their large orbit width over a strongly sheared radial electric field. As can be observed on Fig.1b, the time evolution of the precessional frequency of linearly resonant EPs plus the perturbed $E \times B$ frequency at $\rho = \rho_{q_{min}}$ matches almost exactly the time evolution of the fishbone frequency with zonal flows, which explains why the phase space structure in the trapped region remains static. The strongly sheared $E \times B$ poloidal flow can also perturb the EPs transit frequencies due to their large orbit width, leading to a resonance detuning and the disappearance of the $\omega = \omega_\zeta - \omega_b$ hole and clump. Zonal flows are therefore able to dominate the fishbone saturation by strongly reducing the resonant wave-particle trapping.

Fishbone-induced ion ITB formation - On top of affecting the fishbone mode mitigation, the zonal flows also generate a strong shearing rate within $\rho_T \in [0.1, 0.5]$ with $\gamma_E \sim 3 \times 10^5 \text{ s}^{-1}$. High-n electrostatic GTC simulations with kinetic trapped electrons were performed for this DIII-D configuration, finding that the most unstable drift-wave is a TEM mode at $\rho = 0.4$, shown on Fig.4a, with a linear growth rate of $\gamma_{TEM} = 1.38 \times 10^5 \text{ s}^{-1}$. The shearing rate being larger than the TEM growth rate, as displayed on Fig.4b, the simulated fishbone mode could then lead to turbulence modulation by suppression the TEM growth through zonal flows [11], confirming the speculated role of fishbones in the emergence of ITBs [22]. This modulation is supported experimentally in DIII-D by the charge exchange recombination spectroscopy diagnostic. The formation of an ion ITB after fishbone bursts occurring at $t=1581, 1594, 1607$ and 1615ms can indeed be observed on Fig.4 c. The core-increase of T_i cannot be explained by additional heating from the beam, as it was at constant power since $t=300\text{ms}$, multiple slowing-down times before the onset of fishbones. Fishbone bursts were also observed to precede ion-ITB in four others DIII-D discharges with similar heating power, density, current and q_{min} parameters. Electrons are not affected by the ITB, as zonal flows are only able to mitigate ion-scale turbulence [42].

EP transport in ITER prefusion baseline - The GTC code having been nonlinearly validated for fishbone simulations, it can now be applied to the selected ITER scenario to predict the fishbone-induced EP transport. Similar to the DIII-D simulations, the NBI beam is reproduced from an analytical anisotropic slowing-down distribution.

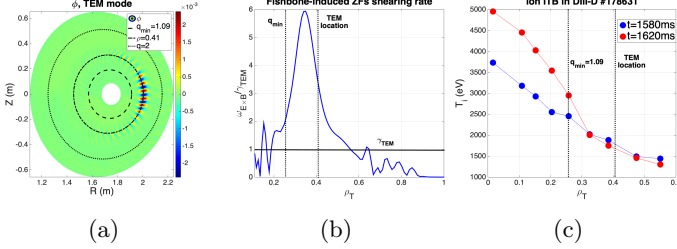


Figure 4: a) Electrostatic potential ϕ of unstable TEM mode in the poloidal plane b) Fishbone-induced shearing rate profile after saturation c) T_i profiles in eV before and after fishbone bursts from charge exchange recombination spectroscopy, exhibiting an ion-ITB.

Linear GTC simulations show that the configuration is unstable to the $n=1$ fishbone with the realistic beam, with a mode growth rate and frequency of $\gamma = 4.4 \times 10^4 \text{ s}^{-1}$ and $\omega/2\pi = 48 \text{ kHz}$, while simulations with equivalent Maxwellian distributions find a configuration stable to $n=1$ modes.

Similarly to DIII-D based simulations, the zonal flows inclusion lowers the $n=1$ mode saturation. The zonal electric field also peaks with negative values close to the q_{min} surface, with a subdominant positive layer further in the plasma. Electrostatic GTC simulations were also performed for this ITER scenario, finding an unstable TEM mode at $\rho = 0.71$ with $\gamma_{TEM} = 3 \times 10^4 \text{ s}^{-1}$. At that location, the fishbone-induced shearing rate is three times larger than the TEM linear growth rate, suggesting that an ion-ITB can also be triggered for this ITER scenario.

However after saturation with zonal flows, the $n=1$ mode abruptly explodes. This numerical instability is due to how zonal flows are computed in GTC. The flux-surface averaged potential ϕ_{00} is computed over the equilibrium flux surfaces, which can be a strong assumption in the nonlinear fishbone phase as $\delta B/B$ grows. This computation will soon be modified to include the perturbed flux surface to enable long time cross-scale simulation between microturbulence and MHD modes with GTC. The study of the fishbone-induced EP transport for that scenario is then conducted without the inclusion of zonal flows to achieve a long nonlinear phase. The transport level will then represent the upper-bound as zonal flows decrease it significantly.

After the end of the fishbone burst, the overall redistribution within q_{min} is of order 2% of the initial distribution, with both inward and outward EP fluxes due to positive and negative EP equilibrium pressure gradient. Such a redistribution tends to marginally flatten the initial pressure gradient, the NBI pressure drive being too low to cause large redistribution. Overall, the NBI fishbone should not impact significantly the plasma heating of this ITER baseline pre-fusion, similar to what was shown for the alpha-fishbone in the ITER 15MA baseline DT scenario [19].

Conclusion - Since fishbone oscillations may not cause significant EP redistribution in ITER plasmas, it can be of great interest to design ITER scenarios to trigger them on purpose rather than avoiding them. As was shown in this Letter, fishbones can generate zonal flows which present two advantages : 1) mitigating the fishbone saturation and its impact on EP transport and 2) creating strong shearing rates that can damp drift-wave instabilities and hence reducing the turbulent transport. While it was observed here and in several tokamak discharges [23][24][43][26][27][25] that fishbone oscillations led to ITBs formation, that was not the case in some others such as JET [44][45][42], despite efforts to reproduce the fishbone-induced ITB formation observed in ASDEX plasmas [23]. It may therefore exist a parametric dependency for the fishbone instability that controls the emergence of strongly sheared fishbone-induced zonal flows. The numerical identification and experimental observation of such a dependency could enable the creation of high-performance scenarios, of crucial importance for ITER burning plasmas.

References

- [1] ITER Physics Expert Group on Energetic Drive and ITER Physics Basis Editors. Chapter 5: Physics of energetic ions. *Nuclear Fusion*, 39(12):2471–2495, dec 1999.
- [2] Liu Chen, Zhihong Lin, and Roscoe White. Excitation of zonal flow by drift waves in toroidal plasmas. *Physics of Plasmas*, 7(8):3129–3132, aug 2000.
- [3] Liu Chen and Fulvio Zonca. Nonlinear excitations of zonal structures by toroidal alfvén eigenmodes. *Physical Review Letters*, 109(14):145002, oct 2012.
- [4] Liu Chen and Fulvio Zonca. Physics of alfvén waves and energetic particles in burning plasmas. *Reviews of Modern Physics*, 88(1):015008, mar 2016.
- [5] Z. Qiu, L. Chen, and F. Zonca. Effects of energetic particles on zonal flow generation by toroidal alfvén eigenmode. *Physics of Plasmas*, 23(9):090702, sep 2016.
- [6] Z. Lin, T. S. Hahm, W. W. Lee, W. M. Tang, and R. B. White. Turbulent transport reduction by zonal flows: Massively parallel simulations. *Science*, 281(5384):1835–1837, sep 1998.
- [7] Y. Todo, H.L. Berk, and B.N. Breizman. Saturation of a toroidal alfvén eigenmode due to enhanced damping of nonlinear sidebands. *Nuclear Fusion*, 52(9):094018, sep 2012.
- [8] Huasen Zhang and Zhihong Lin. Nonlinear generation of zonal fields by the beta-induced alfvén eigenmode in tokamak. *Plasma Science and Technology*, 15(10):969–973, oct 2013.

[9] Y. Chen, G. Y. Fu, C. Collins, S. Taimourzadeh, and S. E. Parker. Zonal structure effect on the nonlinear saturation of reverse shear alfvén eigenmodes. *Physics of Plasmas*, 25(3):032304, mar 2018.

[10] H.W. Zhang, Z.W. Ma, J. Zhu, W. Zhang, and Z.Y. Qiu. Zonal flow generation and toroidal alfvén eigenmode excitation due to tearing mode induced energetic particle redistribution. *Nuclear Fusion*, 62(2):026047, jan 2022.

[11] T. S. Hahm and K. H. Burrell. Flow shear induced fluctuation suppression in finite aspect ratio shaped tokamak plasma. *Physics of Plasmas*, 2(5):1648–1651, may 1995.

[12] G. D. Conway, D. N. Borba, B. Alper, D. V. Bartlett, C. Gormezano, M. G. von Hellermann, A. C. Maas, V. V. Parail, P. Smeulders, and K-D. Zastrow. Suppression of plasma turbulence during optimized shear configurations in JET. *Physical Review Letters*, 84(7):1463–1466, feb 2000.

[13] A Di Siena, R Bilato, T Grler, E Poli, A Bañón Navarro, D Jarema, and F Jenko. Core transport barriers induced by fast ions in global gyrokinetic GENE simulations. *Plasma Physics and Controlled Fusion*, 64(6):064003, may 2022.

[14] K. McGuire and al. Study of high-beta magnetohydrodynamic modes and fast-ion losses in PDX. *Physical Review Letters*, 51(20):1925–1925, nov 1983.

[15] Liu Chen, R. B. White, and M. N. Rosenbluth. Excitation of internal kink modes by trapped energetic beam ions. *Physical Review Letters*, 52(13):1122–1125, mar 1984.

[16] J. Candy, H. L. Berk, B. N. Breizman, and F. Porelli. Nonlinear modeling of kinetic plasma instabilities. *Physics of Plasmas*, 6(5):1822–1829, may 1999.

[17] A. Ödblom, B. N. Breizman, S. E. Sharapov, T. C. Hender, and V. P. Pastukhov. Nonlinear magnetohydrodynamical effects in precessional fishbone oscillations. *Physics of Plasmas*, 9(1):155–166, jan 2002.

[18] G. Y. Fu, W. Park, H. R. Strauss, J. Breslau, J. Chen, S. Jardin, and L. E. Sugiyama. Global hybrid simulations of energetic particle effects on the $n=1$ mode in tokamaks: Internal kink and fishbone instability. *Physics of Plasmas*, 13(5):052517, may 2006.

[19] G. Brochard, R. Dumont, H. Lütjens, X. Garbet, T. Nicolas, and P. Maget. Nonlinear dynamics of the fishbone-induced alpha transport on ITER. *Nuclear Fusion*, 60(12):126019, oct 2020.

[20] A.R. Polevoi, A.A. Ivanov, S.Yu. Medvedev, G.T.A. Huijsmans, S.H. Kim, A. Loarte, E. Fable, and A.Y. Kuyanov. Reassessment of steady-state operation in ITER with NBI and EC heating and current drive. *Nuclear Fusion*, 60(9):096024, aug 2020.

[21] Wanling Ge, Zheng-Xiong Wang, Feng Wang, Zixi Liu, and Liqing Xu. Multiple interactions between fishbone instabilities and ITBs in EAST plasmas. *Nuclear Fusion*, nov 2022.

[22] S. D. Pinches, S. Günter, and A. G. Peeters. Fishbone generation of sheared flows and the creation of transport barriers. *28th EPS Conference on Contr. Fusion and Plasma Phys. (Funchal) Vol 25A p 57*, 2001.

[23] S Günter, A Gude, J Hobirk, M Maraschek, S Saarelma, S Schade, R.C Wolf, and ASDEX Upgrade Team. MHD phenomena in advanced scenarios on ASDEX upgrade and the influence of localized electron heating and current drive. *Nuclear Fusion*, 41(9):1283–1290, sep 2001.

[24] A.R. Field, C. Michael, R.J. Akers, J. Candy, G. Colyer, W. Guttenfelder, Y. c. Ghim, C.M. Roach, and S. Saarelma and. Plasma rotation and transport in MAST spherical tokamak. *Nuclear Fusion*, 51(6):063006, apr 2011.

[25] C.A. Michael, N.A. Crocker, and J. Hillesheim. Influence of fishbone-induced fast-ion losses on rotation and transport barrier formation in mast. *INIS-XA-21M2910 - International Atomic Energy Agency (IAEA)*, 2019.

[26] Y Yang, X Gao, H Q Liu, G Q Li, T Zhang, L Zeng, Y K Liu, M Q Wu, D F Kong, T F Ming, X Han, Y M Wang, Q Zang, B Lyu, Y Y Li, Y M Duan, F B Zhong, K Li, L Q Xu, X Z Gong, Y W Sun, J P Qian, B J Ding, Z X Liu, F K Liu, C D Hu, N Xiang, Y F Liang, X D Zhang, B N Wan, J G Li, and Y X Wan and. Observation of internal transport barrier in ELM- α mode plasmas on the EAST tokamak. *Plasma Physics and Controlled Fusion*, 59(8):085003, jun 2017.

[27] Xiang Gao. Sustained high 10.1088/1009-0630/15/10/02betan plasmas on EAST tokamak. *Physics Letters A*, 382(18):1242–1246, may 2018.

[28] W.W. Heidbrink, M.A. Van Zeeland, M.E. Austin, N.A. Crocker, X.D. Du, G.R. McKee, and D.A. Spong. Stability of beta-induced alfvén eigenmodes (BAE) in DIII-d. *Nuclear Fusion*, 61(6):066031, may 2021.

[29] W. Deng, Z. Lin, and I. Holod. Gyrokinetic simulation model for kinetic magnetohydrodynamic processes in magnetized plasmas. *Nuclear Fusion*, 52(2):023005, jan 2012.

[30] Yong Xiao, Ihor Holod, Zhixuan Wang, Zhihong Lin, and Taige Zhang. Gyrokinetic particle simulation of

microturbulence for general magnetic geometry and experimental profiles. *Physics of Plasmas*, 22(2):022516, feb 2015.

[31] Ge Dong, Jian Bao, Amitava Bhattacharjee, Alain Brizard, Zhihong Lin, and Peter Porazik. Gyrokinetic particle simulations of the effects of compressional magnetic perturbations on drift-alfvenic instabilities in tokamaks. *Physics of Plasmas*, 24(8):081205, aug 2017.

[32] Chang Liu, Stephen C. Jardin, Hong Qin, Jianyuan Xiao, Nathaniel M. Ferraro, and Joshua Breslau. Hybrid simulation of energetic particles interacting with magnetohydrodynamics using a slow manifold algorithm and gpu acceleration. *Arxiv:2107.13663*, July 2021.

[33] S C Jardin, N Ferraro, J Breslau, and J Chen. Multiple timescale calculations of sawteeth and other global macroscopic dynamics of tokamak plasmas. *Computational Science & Discovery*, 5(1):014002, may 2012.

[34] N.M. Ferraro and S.C. Jardin. Calculations of two-fluid magnetohydrodynamic axisymmetric steady-states. *Journal of Computational Physics*, 228(20):7742–7770, nov 2009.

[35] Hinrich Lütjens and Jean-François Luciani. The XTOR code for nonlinear 3d simulations of MHD instabilities in tokamak plasmas. *Journal of Computational Physics*, 227(14):6944–6966, jul 2008.

[36] Hinrich Lütjens and Jean-François Luciani. XTOR-2f: A fully implicit newton–krylov solver applied to nonlinear 3d extended MHD in tokamaks. *Journal of Computational Physics*, 229(21):8130–8143, oct 2010.

[37] G. Brochard, R. Dumont, H. Lütjens, and X. Garbet. Linear stability of the ITER 15 MA scenario against the alpha fishbone. *Nuclear Fusion*, 60(8):086002, jul 2020.

[38] G. Brochard, J. Bao, C. Liu, N. Gorelenkov, G. Choi, G. Dong, P. Liu, J. Mc.Clenaghan, J.H. Nicolau, F. Wang, W.H. Wang, X. Wei, W.L. Zhang, W. Heidbrink, J.P. Graves, Z. Lin, and H. Lütjens. Verification and validation of linear gyrokinetic and kinetic-MHD simulations for internal kink instability in DIII-d tokamak. *Nuclear Fusion*, 62(3):036021, jan 2022.

[39] Dmitry Moseev and Mirko Salewski. Bi-maxwellian, slowing-down, and ring velocity distributions of fast ions in magnetized plasmas. *Physics of Plasmas*, 26(2):020901, feb 2019.

[40] M. N. Rosenbluth and F. L. Hinton. Poloidal flow driven by ion-temperature-gradient turbulence in tokamaks. *Physical Review Letters*, 80(4):724–727, jan 1998.

[41] F. L. Hinton, J. Kim, Y.-B. Kim, A. Brizard, and K. H. Burrell. Poloidal rotation near the edge of a tokamak plasma in h mode. *Physical Review Letters*, 72(8):1216–1219, feb 1994.

[42] R C Wolf. Internal transport barriers in tokamak plasmas. *Plasma Physics and Controlled Fusion*, 45(1):R1–R91, nov 2003.

[43] W. Chen, Y. Xu, X.T. Ding, Z.B. Shi, M. Jiang, W.L. Zhong, and X.Q. Ji and. Dynamics between the fishbone instability and nonlocal transient transport in HL-2a NBI plasmas. *Nuclear Fusion*, 56(4):044001, mar 2016.

[44] R C Wolf, O Gruber, M Maraschek, R Dux, C Fuchs, S Gnter, A Herrmann, A Kallenbach, K Lackner, P J McCarthy, H Meister, G Pereverzev, J Schweinzer, U Seidel, and the ASDEX Upgrade Team. Stationary advanced scenarios with internal transport barrier on ASDEX upgrade. *Plasma Physics and Controlled Fusion*, 41(12B):B93–B107, dec 1999.

[45] E Joffrin, G Gorini, C D Challis, N C Hawkes, T C Hender, D F Howell, P Maget, P Mantica, D Mazon, S E Sharapov, G Tresset, , and contributors to the EFDA-JET Workprogramme. Triggering of internal transport barrier in JET. *Plasma Physics and Controlled Fusion*, 44(8):1739–1752, aug 2002.